Ultrasonics 99 (2019) 105945

Contents lists available at ScienceDirect

Ultrasonics

journal homepage: www.elsevier.com/locate/ultras

The effect of EMAT coil geometry on the Rayleigh wave frequency behaviour

C.B. Thring, S.J. Hill, S. Dixon, R.S. Edwards*

Department of Physics, University of Warwick, Coventry CV4 7AL, United Kingdom

ARTICLE INFO

Keywords:
Electromagnetic acoustic transducer
Frequency
Rayleigh wave

ABSTRACT

Understanding of optimal signal generation and frequency content for electromagnetic acoustic transducers (EMATs) is key to improving their design and signal to noise ratio. Linear and meander coil designs are fairly well understood, but other designs such as racetrack or focused coils have recently been proposed. Multiple transmission racetrack coil EMATs, with focused and unfocused designs, were constructed. The optimum driving frequency for maximum detected signal was found to range between 1.1 and 1.4 MHz on aluminium for a 1.5 mm width coil. A simple analytical model based on the instantaneous velocity of a wave predicts a maximum signal at 1.44 MHz. Modelling the detection coil as a spatial square wave agrees with this, and predicts a general relation of $f_P = 0.761v/L$ between the optimum frequency f_P, the wave velocity v, and the coil width L. A time domain model of the detection coil predicts a 1.4–1.5 MHz peak for continuous wave excitation, with a frequency that decreases as the length of the wavepacket is decreased, consistent with the experimental data. Linear coil modelling using the same technique is shown to be consistent with previous work, with improving detection at lower wave frequencies, and signal minima at every integer multiple of the wavelength. Finite Element Analysis (FEA) is used to model the effects of the spatial width of the racetrack generation coil and focused geometry, and no significant difference is found between the focused and the unfocused EMAT response. This highlights the importance of designing the EMAT coil for the correct lift-off and desired frequency of operation.

1. Introduction

Electromagnetic acoustic transducers (EMATs) are of use for non-destructive testing (NDT) in industry due to their ability to work in harsh environments [1]. A typical EMAT consists of a coil backed by a permanent magnet, as shown in Fig. 1(a). They generate ultrasound directly in surface near zones of electrically conductive materials, allowing them to function without couplant and without contacting the sample, allowing for fast scanning [2–4]. EMATs can be used at high temperatures, with the temperature of operation limited by the Curie temperature of the magnet needed for detection and/or any cooling mechanisms [5,6]. However, the generation mechanism is inefficient, and EMATs can suffer from low signal to noise ratios (SNR) [7].

Increasing safety requirements in industry are putting more emphasis on early stage detection of defects [8]. For small surface-breaking defects, a high frequency (short wavelength) Rayleigh wave can be appropriate for detection [9,10]. The frequency of the Rayleigh wave generated or detected by an EMAT is dependent on the geometry of the coil, with a higher frequency wave requiring a narrower coil width [11]. Full understanding of the frequency behaviour of EMATs is therefore essential to improving and optimising their capabilities.

EMATs can be designed with different coil designs and magnet configurations, depending on the type of wave generation required and the application [1,12–18]. The coil geometry used for generating surface waves, such as linear (Fig. 1(a)), meanderline (Fig. 1(b)), or racetrack (Fig. 1(c)), puts a limitation on the maximum frequency that can be feasibly generated and detected [11,19]. For meanderline coils the spacing between the turns sets a wavelength, which tunes the EMAT to work well around a chosen frequency. For the linear coil, the coil width determines the frequency sensitivity [11]. A very narrow detection coil increases the frequency limit, however, the narrower the coil, the weaker the detected signal amplitude.

Recent research has suggested the use of geometric focusing as a method to improve the signal strength and spatial resolution of EMATs [9,13,14,20]. Meanderline designs were produced with spacing to generate signals with a maximum of 2 MHz, and the generated and detected frequencies were as expected [9]. However, the frequencies produced by similar focused racetrack designs were not as predicted, based on the linear coil model [11,20].

This work details the analytical solutions for the expected

* Corresponding author.
E-mail address: r.s.edwards@warwick.ac.uk (R.S. Edwards).

https://doi.org/10.1016/j.ultras.2019.06.007
Received 13 November 2018; Received in revised form 2 June 2019; Accepted 10 June 2019
Available online 12 June 2019

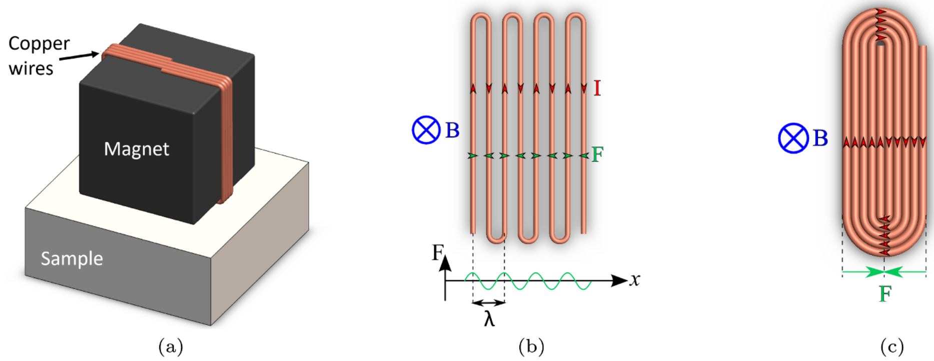

Fig. 1. (a) Linear coil EMAT. (b) Meanderline EMAT wire coil schematic with forces shown for an external magnetic field. Sometimes multiple turns of thinner wire are wound through the same meander pattern instead of the single wire shown to improve current density. (c) Racetrack EMAT coil schematic and forces.

operational frequencies of racetrack coils, and presents experimental work using both focused and unfocused racetrack coils. Models are presented to explain the discrepancies between the analytical and the experimental results. Finite element modelling is used to investigate the difference between focused and unfocused designs, and the effect of the frequencies generated vs. the detection capabilities. Predictions are given for how to design an EMAT optimised for a chosen frequency range.

2. Methodology

The main (unfocused) EMAT designs used in this work are shown in Fig. 1. All the EMATs used contain a permanent magnet as shown in Fig. 1(a); for the meanderline and racetrack designs just the coil is shown for clarity. As a large magnetic field from the permanent magnet is used, the Lorentz force from the alternating magnetic field (or self-field) created by the alternating current pulse is neglected for the levels of current used in these experiments [21]. All of the racetrack and linear designs operate in transmission mode. For this, separate generation and detection coils are used, held a fixed separation apart [20]. The detection coil picks up the signal transmitted directly along a sample containing no defects. The focused meanderline EMATs included for comparison are a pseudo-pulse-echo design, using two coils in close proximity as a 'send' and 'receive' coil to measure reflections from defects [9]. Its frequency capabilities were tested by analysing a reflection from the end of a billet, representing an 'infinite' depth defect.

For all experiments an aluminium billet was used as a sample, with a thickness of at least several wavelengths. An adapted Ritec RAM-5000 pulser was used to allow generation of a set number of cycles at a chosen frequency; this system is optimised for high frequency (1–20 MHz) operation. A three cycle sinusoid was used to excite all racetrack designs. Detected signals from a preamplifier connected to the detection EMAT were recorded on an oscilloscope. Analytical calculations and finite element analysis (FEA) modelling using the software PZFlex, were carried out to understand the frequency behaviour of the racetrack coil designs.

Several different designs of coil were used for the experiments. For the racetrack coils, two separate sets of focused 1.5 mm width coils were produced, as shown in Fig. 2(a). The second was an attempt at an identical repeat, to test reproducibility. A third focused set with the coil width reduced to 0.75 mm was also produced. Two unfocused racetrack pairs (Fig. 2(b) & (c)) were designed and built, with one set designed to be longer to include the effect of increasing resistance. The magnet indicated in the figure has a height of 25 mm, and is a grade N45 NdFeB permanent magnet. Its shape is optimised for the focused coils, and so the unfocused coil pair (b) was also tested using a pair of 10 × 25 × 10 mm cuboidal magnets. Further details on the focused design can be found in reference [20].

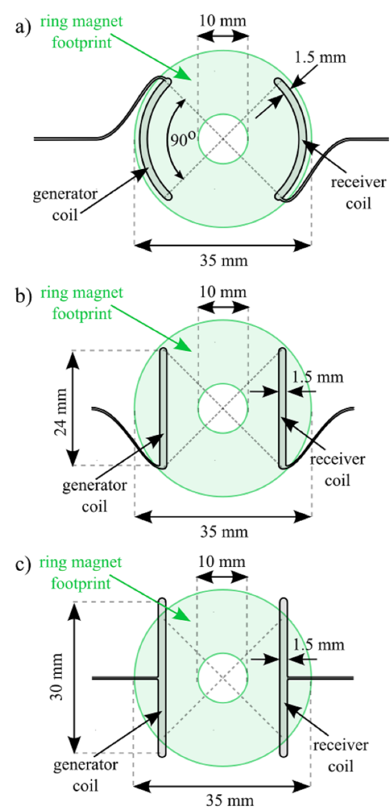

Fig. 2. (a) Focused racetrack EMAT transmission coil pair, (b) unfocused racetrack comparative coil pair, (c) unfocused longer coil pair.

3. Analytical solutions

Meanderline coils, as shown in Fig. 1(b), have a very simple relationship between design and their optimum generation and detection frequency, as the meander turns are designed to match the wavelength of the desired wavefront when operated with a large bias magnetic field [19]. Meanderline coils can operate at high frequencies by using individual turns that are narrow, but they circumvent the problem of reduced signal strength by having multiple turns. Further tuning of the frequency behaviour is possible by using capacitors to tune the electrical impedance [1,9]. However, this gives a narrowband signal, which is not necessarily desirable.

Dixon et al. [11] explore the frequency behaviour for linear coils of finite width, shown in Fig. 1(a), by taking the wave equation

$$A = A_o e^{i(\omega t - kx)}, \quad (1)$$

where A is the wave displacement, A_o is the maximum amplitude, ω is

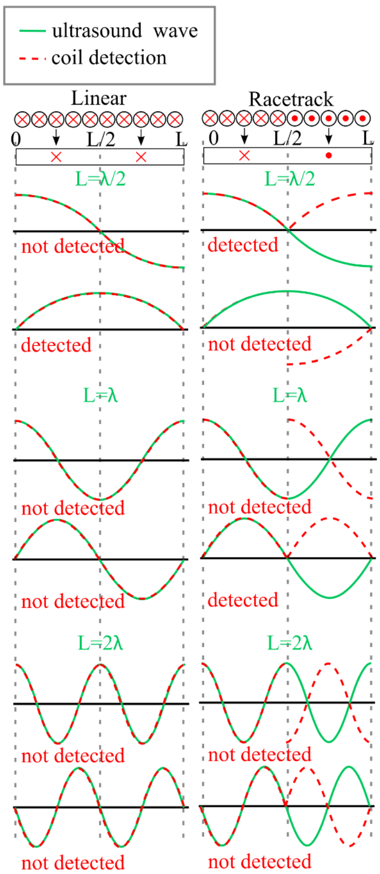

Fig. 3. Comparison of the detection capabilities of linear and racetrack coils for different wavelength and phase waves. The wave is shown as green, and red shows how this is measured by the coil, considering opposing wire directions. (For interpretation of the references to color in this figure legend, the reader is referred to the web version of this article.)

the angular frequency, k is the wavenumber, t is time, and x is the distance propagated. Differentiating with respect to x gives the instantaneous wave velocity v which is detected by the EMATs [11],

$$v = i\omega A_o e^{i(\omega t - kx)}. \tag{2}$$

Integrating this between $-L/2$ and $L/2$ gives the detected signal once it has been averaged over the spatial width of a coil of width L, with 0 at its center. This solves to give a voltage in the detection coil of

$$V_{coil} \propto \frac{-2e^{i\omega t}}{k}\left(\sin\left(\frac{kL}{2}\right)\right). \tag{3}$$

Neglecting time variations, the voltage in the coil is approximated as

$$V_{coil} \propto \frac{1}{k}\sin\left(\frac{kL}{2}\right). \tag{4}$$

Minima in detection will therefore occur when the sine term equates to zero. As $k = 2\pi/\lambda$ minima will be found when

$$L = \frac{2n\pi}{k} = n\lambda, \tag{5}$$

where n is any positive integer. Fig. 3 shows a schematic of the two different coil designs, with a snapshot of the wave behaviour under the coil shown as a green solid line. The detected signal depends on the wave behaviour under the whole coil; as a simplification, it will return the average amplitude of the red dashed line, which considers the wire directions and the Lorentz force detection mechanism. For the linear coil the wires are all in the same direction. Considering the schematic for linear coil detection for $L = \lambda$ and $L = 2\lambda$ for two different phase waves, the detected signal will average to zero; from symmetry the signals detected by the separate wires will always cancel out no matter what the phase is beneath the coil, and the wave will not be detected, in agreement with the equation.

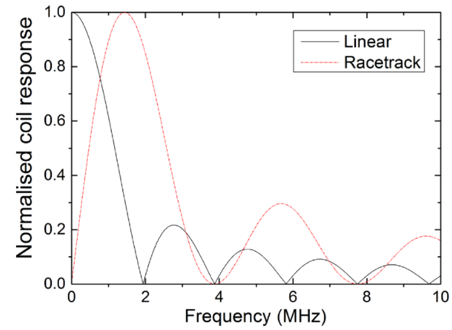

Fig. 4. Analytical solutions to the response of a linear and racetrack EMAT detection coil, both of width 1.5 mm, to ultrasonic signals of different frequencies.

Maxima in detection are shifted from the half integer values of the wavelength due to the $1/k$ term in Eq. (4). This shift can be seen in the peak positions shown in Fig. 4 (solid line), for $v_R = 2906$ m/s (Rayleigh wave velocity in aluminium, used throughout). Again, the shift can be understood intuitively by considering the effect of different phase waves for a coil of width $L = \lambda/2$, as shown in Fig. 3. The detectability of the wave depends on the phase of the wave underneath the coil. It is advisable to design detection linear EMAT coils to have a width equal to or less than half the wavelength of the signal of interest, to ensure sufficient signal is detected [11].

To extend this to racetrack coils, which have opposing current directions in the two halves of the coil, a similar integral can be evaluated considering each half of the coil separately,

$$V_{coil} \propto \int_{-L/2}^{0} e^{i(\omega t - kx)}dx - \int_{0}^{L/2} e^{i(\omega t - kx)}dx. \tag{6}$$

This evaluates to

$$V_{coil} \propto \frac{2ie^{i\omega t}}{k}\left(1 - \cos\left(\frac{kL}{2}\right)\right). \tag{7}$$

Neglecting time variations again gives:

$$V_{coil} \propto \frac{1}{k}\left(1 - \cos\left(\frac{kL}{2}\right)\right). \tag{8}$$

Minima in detection will therefore occur when the $(1 - \cos)$ term equates to zero, i.e. at

$$\frac{kL}{2} = 2n\pi, \tag{9}$$

$$L = \frac{4n\pi}{k} = 2n\lambda. \tag{10}$$

These minima have a similar intuitive explanation to the linear coils, as shown in Fig. 3. A wave with a wavelength of half the coil width will always cancel to give no wave detected, for all phases. As with the linear case, the frequency at which the detected signal is maximum is less clear as phase impacts whether the signal will be detected.

Fig. 4 (red dashed line) shows the absolute value of Eq. (8) for $v_R = 2906$ m/s and $L = 1.5$ mm (total coil width). This clearly shows the first two minima for the racetrack coil as expected at 3.9 and 7.8 MHz. The $1/k$ term shifts the maxima to lower frequencies. In this example the first peak occurs at a frequency of 1.44 MHz, suggesting this as the optimal frequency for operation.

This analytical model gives a useful prediction of the behaviour of a coil of a chosen width L. However, experimental observations initially found that a racetrack coil with a width of 1.5 mm used on aluminium

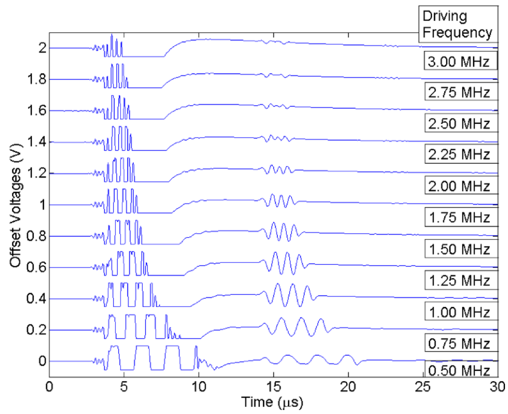

Fig. 5. Detected signals from the 1.5 mm width, focused transmission coils pair with a driving signal of 3 cycles and varied driving frequencies.

had optimal signal generation when a 3 cycle signal of lower frequency (around 1 ± 0.3 MHz) was used to drive the coil [20]. Further consideration must be made of the other factors which affect the frequency behaviour of an EMAT.

4. Experimental results

An example set of A-scans taken using a 1.5 mm wide pair of focused racetrack coils are shown in Fig. 5 for several different driving frequencies [20]. The noise from the driving signal starts at 3.8 μs and saturates the signal amplifier. The Rayleigh wave starts at around 15 μs. The analytical calculations suggest that the maximum signal should be observed at 1.44 MHz. The peak-to-peak (p-p) voltage for the Rayleigh waves was measured as a function of driving frequency for all coils used, and is shown in Fig. 6. The fits shown and used to estimate the peak locations are cubic splines, with a peak location error of ± 0.13 MHz from the data resolution. Overall, the driving frequencies that gave the strongest signals ranged from 1.1 MHz to 1.4 MHz for the 1.5 mm width racetrack coils. These values are recorded in Table 1 in the column ‘Driving Frequency for Max Signal’. These are consistently lower than predicted by the analytical model.

Experimental factors that might affect the frequency response of a coil are the electrical impedance of the coil and the system, the lift-off between the coil and the sample, and the accuracy of producing and measuring the coil width. All coils used are hand wound using 0.08 mm diameter wire. All the racetrack coil widths were measured using an optical microscope at three positions along their length and the average taken to account for minor variations. Table 1 gives the measured widths of both the generation and the detection coil for each pair, separated by commas, in the column ‘Measured Coil Width’. The expected optimum frequency for the strongest generated signal from the

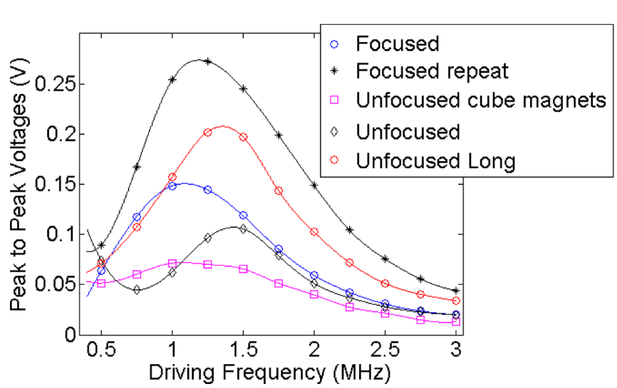

Fig. 6. Output maximum peak to peak signal found for multiple 1.5 mm width racetrack coils.

Table 1
EMAT designs and frequency response behaviour. ‘Measured Coil Width’ gives both the generator and the detector coils. The ‘Theoretical Frequency Peak’ gives the frequency at which a maximum is predicted by the analytical calculations in Section 3.

Coil type	Designed coil width (mm)	Measured coil width (mm)	Theoretical frequency peak (MHz)	Driving frequency for max signal (MHz)	Detected frequency of max signal (MHz)
Unfocused Meaderline	6 × 1.5 meanders	–	1.9	1.8	1.6
Focused Meaderline	6 × 1.5 meanders	–	1.9	1.9	1.7
Focused	1.5	1.46, 1.53	1.48, 1.41	1.1	1
	1.5 (rep)	1.54, 1.43	1.40, 1.51	1.2	0.99
Racetrack	0.75	0.70, 0.62	3.08, 3.48	2.25	2.23
Unfocused	1.5	1.33, 1.19	1.62, 1.81	1.4	1.25
Racetrack	1.5 long	1.43, 1.52	1.51, 1.42	1.4	1.02
Focused Linear	0.75	–	0	0.6	0.57

analytical calculations based on the measured coil width is given in the column ‘Theoretical Frequency Peak’. Some variation in peak frequency is expected from variations in the coil widths, however, they are mostly under the designed width which should increase the peak frequency of the Rayleigh wave, not decrease it. All racetrack coils were measured using an impedance analyser and found to have resonant frequencies around 40 MHz as they create a single-component L-R resonant circuit, but this is much higher than the driving frequencies, and so resonant effects cannot be altering the operation.

The current output of the Ritec was measured by attaching a set of parallel resistors to the return ground in the coaxial cable and measuring the voltage drop over them, giving the output voltage within the 10% tolerance of the resistors. Example data for the focused racetrack pair is shown in Fig. 7. The Ritec output increases as the frequency is increased, leading to an overestimate of the frequency values from Fig. 6. However, the slope in Fig. 7 is gradual, so it does not make a large difference to the peak positions. The frequency response of the amplifiers used in conjunction with the EMAT detectors was also checked and found to have no measurable variation until well above the frequency range being used.

As the driving frequency was increased from 0.5 to 1.0 MHz, the Rayleigh wave had a peak in its fast Fourier transform (FFT) at a frequency that matched the driving frequency, as shown in Fig. 8 for the 1.5 mm focused racetrack pair. However, as the driving frequency was increased beyond 1 MHz, the frequency of the peak output from the FFT started to fall short of the driving frequency. It can be seen in Fig. 8 that the FFTs contain side lobes. At driving frequencies above 2.25 MHz for

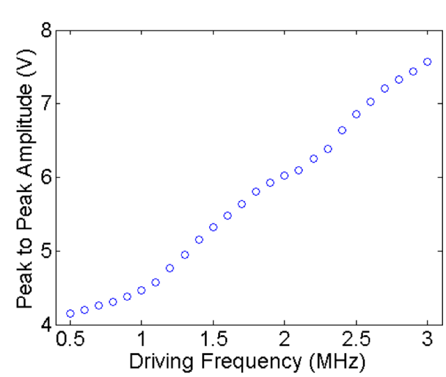

Fig. 7. The peak to peak amplitude of the voltage drop measured over the Ritec ground over a set of parallel resistors making a 1 Ω load together while the frequency is varied to test the focused racetrack EMAT shown in Fig. 2(a).

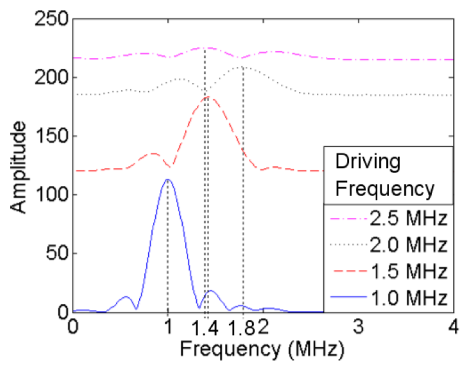

Fig. 8. The frequency content of four example signals shown in Fig. 5 for the focused 1.5 mm racetrack coil pair.

the 1.5 mm width racetrack coils the signals at the driving frequency are small, and the measured frequency of the peak signal becomes dominated by a lower frequency side lobe.

The frequency of the Rayleigh wave measured when the driving frequency is such that the time signal has maximum amplitude is included in the column 'Detected Frequency of Max Signal'. For reference Table 1 also contains the corresponding data for a thinner, focused racetrack coil, 0.75 mm in width, a focused linear coil, also 0.75 mm in width operating in transmission, and a pair of reflection meanderline coils [9]. The meander coils show a FFT peak close to the designed frequency irrespective of driving frequency over a wide driving frequency range, due to the use of tuning (capacitors and coil design).

5. Modelling

Several models are put forward to investigate the discrepancy between the optimal frequencies predicted by the analytical solutions and the experimental results. The first considers the coil spatial width. Other models consider electromagnetic effects due to lift-off between coil and sample [22], and the effect of the phase of the wave on detection. Finally, FEA is used to study both the generator and the detector spatial effects, and the difference between focused and unfocused designs.

5.1. Spatial frequency model

The detected signal from an EMAT coil should be the convolution of the frequency of the signal it is trying to detect, and the frequency profile arising from the spatial width of the coil [11,1]. Three models for the spatial detection capabilities of a racetrack coil are considered. The first is a square wave and assumes equal detection capabilities across the coil. For a 1.5 mm width coil the detectability is set as + 1 over the range 0 to 0.75 mm, and − 1 over the range 0.75 mm to 1.5 mm, matching the assumptions of the analytical model. A more extreme model is to assume detection is only at the center of each side of the coil, i.e. a pair of delta spikes, + 1 at 0.375 mm and − 1 at 1.125 mm. This is a possibility if the magnetic field is weak at the edges, and the opposing wire directions at the center cause a cancellation through their opposing self-field. A compromise between the two models is a single sinusoid across the width.

Taking the FFT of these waves and using $v_R = 2906$ m/s gives the profiles shown in Fig. 9. The first frequency maxima are 1.9 MHz for the delta spikes, 1.7 MHz for the sine wave, and 1.5 MHz for the square wave. All give a minimum at 3.9 MHz which is in agreement with the analytical model. As expected, the square wave model is in the closest agreement with the analytical model.

Calculating the peak frequencies for the square wave model for different coil widths gives a consistent relationship between the width and the frequency at which a maximum amplitude is found in the FFT.

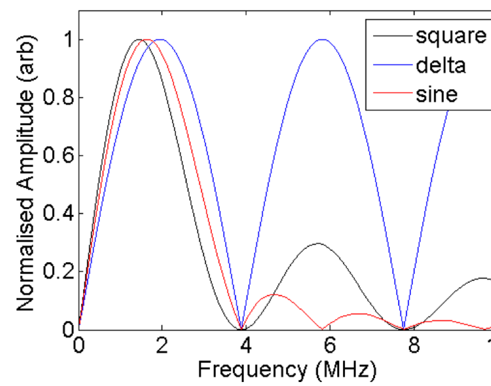

Fig. 9. The FFT for a single cycle square wave, sinusoid, or pair of spikes, for a 1.9 MHz signal.

This relationship is given by

$$f_P = 0.761\frac{v_R}{L}, \tag{11}$$

where L is the full width of the square wave, or the full width of the racetrack coil. Similarly to the analytical model, this allows an upper frequency limit to be predicted for each coil design using the above equation. However, the predictions are higher than the experimental results, and this on its own is not sufficient to fully explain the frequency behaviour.

5.2. Coil-sample lift-off

The distance between the EMAT coils and the sample surface has been minimised, but as the coils are encapsulated in a layer of insulating tape the lift-off from the sample is about 0.1 mm. The electromagnetic field profile seen by the sample will therefore be wider than the coil width, as the electromagnetic field extends beyond the coils. The vector potential A generated in a sample by a ring coil has been found by Dodd and Deeds [23]. Assuming only one substrate ($\alpha_1 = \alpha_2$ in the notation used by Dodd and Deeds) the theory simplifies to the expression

$$A(r, z) = \mu I r_0 \int_0^\infty J_1(ar_0)J_1(ar)e^{-\alpha l}a\left(\frac{e^{\alpha z}}{a + \alpha}\right)da, \tag{12}$$

where r is the radial position from the center of the coil, r_0 is the radius at which the coil is located, z is the vertical distance from the coil, μ is the permeability of the substrate, I is the magnitude of the current pulse in the coil, J_1 is a first order Bessel function, $\alpha = \sqrt{a^2 + i\omega\mu\sigma}$, and σ is the electrical conductivity of the substrate. This can be used to approximately predict the lift-of behaviour of an EMAT coil.

The effect from a whole set of concentric rings can be found by summing the effects from multiple such equations at different locations. Neglecting self-field effects, the vector potential is proportional to the current induced in the sample (Fig. 10(a)). Summing this through the skin depth of the sample gives a surface profile proportional to the current in the sample surface (Fig. 10(b)). Taking the FFT of this profile, and converting to a frequency using v_R gives another theoretical measure of the frequency content from the coil spatial profile and how this varies with lift-off. While this is designed for a pancake coil, the 2D cross-section through the coils will look similar to a racetrack. A 1.5 mm diameter coil creates a profile with a peak in the FFT magnitude at 1.35 MHz. At 0.1 mm lift-off this drops to 1.29 MHz, as shown in Fig. 10(c). Whilst these numbers are lower than those seen experimentally, this is due to the inaccuracies in the model, but the behaviour with lift-off is shown to reduce the frequency. It is therefore possible that lift-off effects partly account for the lower frequencies seen. However, it is not enough of a drop to account for all the data, especially when the effect of the increasing Ritec current with frequency is

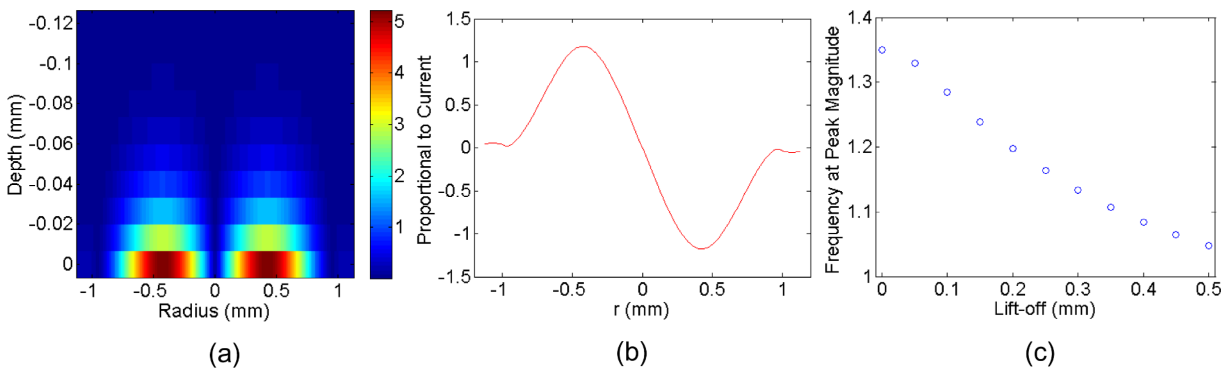

Fig. 10. (a) Example current density profile in an Aluminium substrate, 0.1 mm below a pancake coil of radius 0.75 mm with a continuous AC of frequency 1.285 MHz (color bar values are proportional to the current density). (b) the surface current profile from the same coil. (c) the frequency at which a peak is found in the magnitude of the FFT of profiles such as the one in (b) with varied separation from the pancake coil. (For interpretation of the references to color in this figure legend, the reader is referred to the web version of this article.)

added.

5.3. Time evolution

To study the effect of a wave travelling under a coil and different signal shapes on detection, a synthetic wave, G, was generated using

$$G = Re\left[e^{\frac{-(t-t_0)^2}{2a^2}} e^{2i\pi f(t-t_0)}\right], \tag{13}$$

where t_0 is the time at which the center of the signal packet occurs and a is the width of the signal in the time domain. This was chosen to match the waves generated in the experiments, where the frequency of the wave and the number of cycles (effectively the envelope length) are set using the Ritec. This wave was evaluated over a time range of 0 to 15 µs with $t_0 = 5$ µs. f was varied from 0.4 to 10 MHz in steps of 0.1 MHz. To test a signal approximating a continuous wave the entire first exponential term that creates the wavepacket was removed, leaving just a cosine signal. To an opposite extreme a was varied as $1/f$, $1/(2f)$, $1/(4f)$, $1/(8f)$, and $1/(16f)$, making the envelope increasingly narrow and giving an increasingly broadband signal. A value of $a = 1/f$ creates a signal with three main significant peaks to match the experimental work. The calculated G signals are shown for f = 1 MHz in Fig. 11(a). The FFTs of the G signals are shown in Fig. 11(b). As the signal becomes closer to a delta-like signal the frequency content moves to peak at 0 MHz for all input f values, and increasing f increases the bandwidth rather than shifting the peak location.

The racetrack coil was modeled by considering a spatial range of 0 to 1.5 mm with increments of 0.1 mm, as a reasonable approximation to the wire diameter and spacing. At each spatial step the synthetic wave G was delayed by a time given by the wire spacing divided by the Rayleigh wave velocity. This is shown schematically with greatly exaggerated delays in the top half of Fig. 12. It was then approximated that the EMAT coil would measure the signal underneath the whole coil instantaneously, and so a single detected signal was generated by summing all the data over the positions 0 to 0.75 mm, and the data over 0.75 to 1.5 mm at each time instance. The second half was subtracted from the first half to account for the change in direction of the wire. This time staggering includes the effect of the variation in the signal detected by each wire over a finite coil width at a single time, creating a simulated 'detected' signal from this superposition, as shown in Fig. 12.

Some example results of the relation between the input signal and the detected signal are shown in Fig. 13, for simulated data with $a = 1/f$, at three different frequencies; 1, 4, and 6 MHz. The 1 MHz detected signal shows very similar amplitudes to the input signal, and the 6 MHz detected signal, while smaller in amplitude, is similar in shape to the input signal. The 4 MHz signal, however, shows a greatly

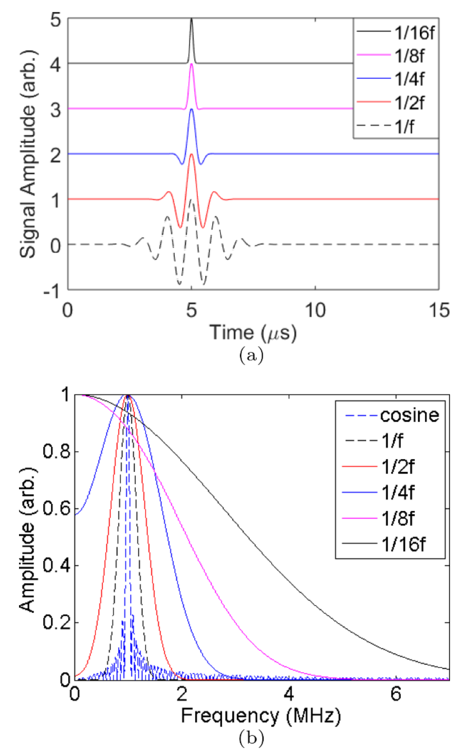

Fig. 11. Synthetic waves with $f = 1$ MHz and an envelope width varied as indicated by the legend. (a) Shows the generated signal G. (b) Shows the FFT data, including the continuous wave for reference. The signals have all been individually normalised.

distorted signal shape, as expected for this detector width as this is near a predicted minimum.

Fig. 14 shows the FFTs of the signals in Fig. 13. The 4 MHz input data shows that the signal has distorted such that it has no 4 MHz signal content. Fig. 15 shows similar FFT data for a bandwidth of $1/(8f)$. As the input signal is now close to a single delta spike there is a large amount of low frequency content, and increasing the frequency broadens the frequency content. The FFTs are close to the full frequency response of the coil spatial width, showing the expected minima and maxima.

To compare the differences caused by varying both f and a, Fig. 16(a) shows the maximum peak to peak signal of the synthetic detected signal s (e.g. the red signals in Fig. 13) for each value of f input into the equation for G, all normalised with respect to the maximum peak to peak signal from the continuous wave (cosine) data for comparison. The minima are in agreement with the analytical calculations.

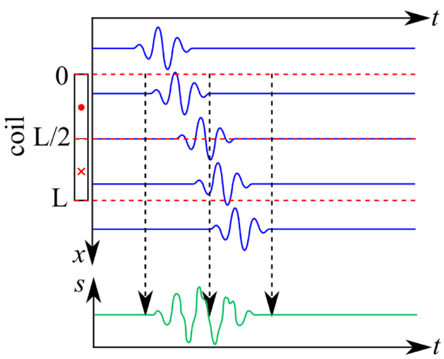

Fig. 12. An arbitrary synthetic signal is shown in blue. As it travels in x its arrival time becomes correspondingly delayed. The actual signal detected by an EMAT coil is the superposition of these signals, s, shown in green. (For interpretation of the references to color in this figure legend, the reader is referred to the web version of this article.)

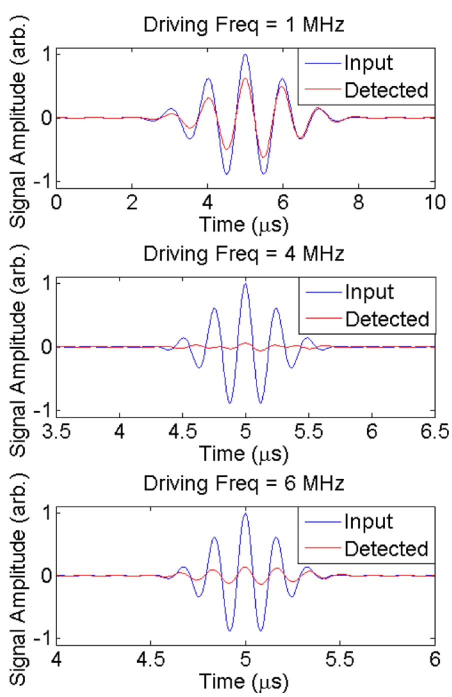

Fig. 13. Example G signals (blue) and synthetic detected signals s (red) from a simulated 1.5 mm width racetrack coil all with an envelope width of the inverse of the frequency. The top graph shows an input frequency of 1 MHz into the equation for G, middle shows 4 MHz, and the lower shows 6 MHz. (For interpretation of the references to color in this figure legend, the reader is referred to the web version of this article.)

The continuous wave data has a peak at 1.45 MHz, which is in agreement with the equivalent square wave impulse response model shown in Fig. 9. However, as the signal packet shrinks from the continuous wave, the peak shifts to the left, with the $1/(4f)$ data having a peak at 1.1 MHz.

The detected frequency is a convolution of the input frequency with the coils' square wave spatial profile, but as signal packets decrease in length, the peak frequency is 'blurred' to a lower value by the frequency averaging effect. As the signal becomes close to a delta spike there is always a strong input frequency content below 4 MHz, meaning that this part of the coil's frequency profile remains dominant over the high frequency peaks, as shown in Fig. 15. Therefore, the curves for the $1/(4f)$, $1/(8f)$, and $1/(16f)$ data in Fig. 16(a) have no distinct minima at 4 and 8 MHz, but simply a gradual decrease in amplitude.

The same program has been run considering instead a linear coil,

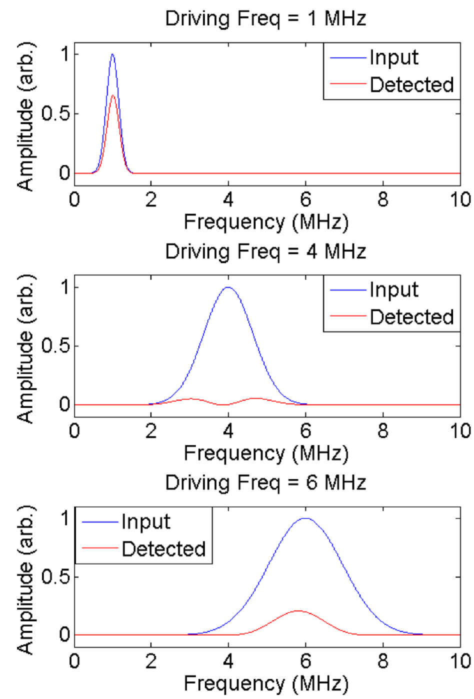

Fig. 14. The output data from taking the FFTs of all the signals shown in Fig. 13.

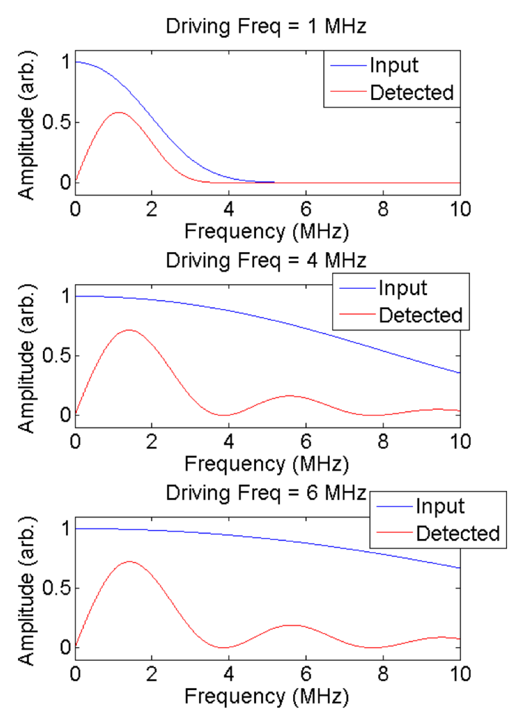

Fig. 15. The FFT data for both the input G signal (blue), and the synthetic detected signals (red) for input frequencies of 1, 4 and 6 MHz, with an envelope width of $1/(8f)$. (For interpretation of the references to color in this figure legend, the reader is referred to the web version of this article.)

where all data between 0 and 1.5 mm is summed at each instant in time. A similar effect is seen, but with minima at every integer value of the wavelength, corresponding to frequencies of 2, 4, 6, etc. MHz. This is shown in Fig. 16(b). The frequency range used for this work was 0.05 to 5 MHz in increments of 0.05 MHz. This is as expected from the analytical calculations, and shows that this model is valid.

This effect also partially explains the low frequency peaks observed

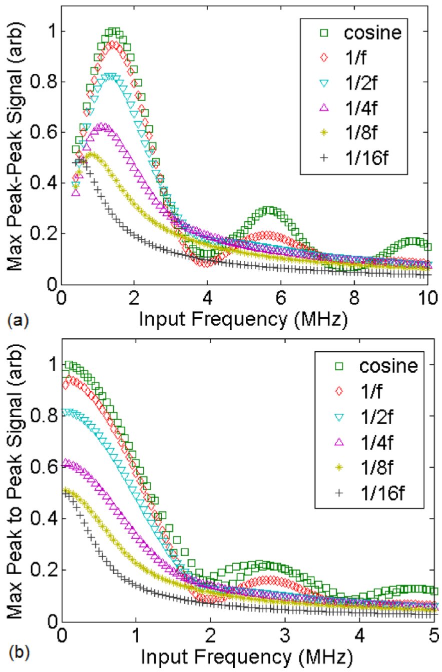

Fig. 16. Normalised maximum peak to peak signal of the detected wave as a function of the frequency input into the synthetic signal, for (a) a 1.5 mm wide racetrack coil, (b) a 1.5 mm wide linear coil.

experimentally, however the drop predicted for $a = 1/f$ is still too small to fully explain the effect. A sufficiently large drop is given by narrower input signals, but these have not been tested experimentally. Considering this alongside the frequency drop created by the coil lift-off could potentially explain the frequency drop. Consideration must also be given to any effects due to the generation coil, or the geometric curvature of the focused EMATs. There is no theoretical reason for this to affect the frequency content, but it could affect the signal phase [24].

5.4. Finite element modelling

A 3D FEA model was developed using the software PZFlex to see if the same frequency lowering effect is seen when considering a finite width generation coil, plus the effects of geometric focusing. All of the models had an element size of 34 µm so that the short wavelengths could be accurately modelled. For generation, a 3 cycle sinusoidal wavefront was applied from every element within the 1.5 mm coil width, with the waveform applied as negative in the second half of the coil to represent the wire directions in a racetrack coil. The driving frequencies of the wavefront were varied from 0.3 to 3 MHz in increments of 0.1 MHz for the focused designs, and from 0.5 to 3 MHz in increments of 0.5 MHz for the unfocused designs to check for consistency.

Fig. 17 shows an example of the simulated x-velocity data at 16.5 mm horizontally away from the coil back edge, for a focused simulation with a driving frequency of 1 MHz. This location is at the designed focal point of the curved design. Fig. 18 shows the maximum peak to peak signal found at the focal point for all the different driving frequencies used for both the focused and the unfocused design, and also for the simulated z displacement data. The peaks found are 2.1 MHz for the x velocity focused simulations, 1.6 MHz for the z displacement focused simulations, 2 MHz for the x velocity unfocused simulations, and 1.5 MHz for the z displacement unfocused simulations. This shows there is some discrepancy between the focused and unfocused simulations, with a slight tendency towards lower frequencies in the unfocused simulations. Discrepancies are likely due to the spreading of the unfocused wavefront as opposed to the coherent

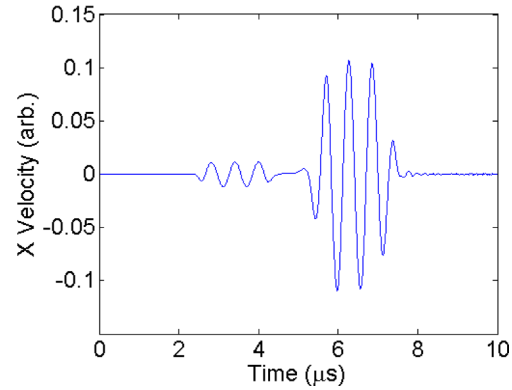

Fig. 17. FEA simulated x-velocity data at 16.5 mm away from the coil back edge, for a driving frequency of 1 MHz. The strongest, later arriving, signal is the three cycle Rayleigh wave; the earlier arriving wave is a surface skimming longitudinal wave.

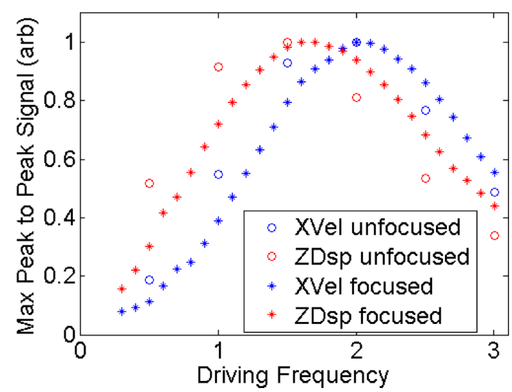

Fig. 18. Maximum peak to peak signal found at the focal point, or equivalent position for the unfocused coils, as a function of the driving frequency using a 1.5 mm racetrack spatial profile. XVel indicates the x direction velocity and ZDsp indicates the z, or out-of-plane displacement.

wavefront seen at the focal point of the focused design, leading to variations in phase as the wave reaches each wire in the coil [24]. In both cases the peak is seen at around 2 MHz for the x velocity data, suggesting the generation is closer to the delta spike model shown in Section 5.1, while the z displacement data is closer to the lower peaks expected from the square wave model. It is as yet unclear why they differ. The Gouy phase shift phenomena might be a factor in the discrepancy [25] as an ultrasonic beam that passes through a focal point will emerge from this with a shift in phase. However, this should not affect the final amplitude at the detection point.

To simulate the racetrack detector, for simplicity just the centerline, $y = 0$, data was considered. The same method as for the time evolution model was then used to simulate a racetrack detector coil; the data between 31.5 and 32.23 mm was summed, and then the sum of the data between 32.25 and 33 mm was subtracted from the first sum to account for the opposing coil directions. The maximum peak-to-peak signal found from this simulated signal is plotted as a function of the driving frequency in Fig. 19. The peaks for all of these are roughly coincident at 1.4 MHz for the z displacement and 1.5 MHz for the x velocity. This indicates that, despite the higher frequency peak seen at the focal point in the x-velocity data, the spatial effect of the detector coil dominates the peak frequency for the whole system, and is in agreement with the continuous wave scenario considered in the previous section. Note that the model does not take into account the wire spacing in the coil, or any variation in this.

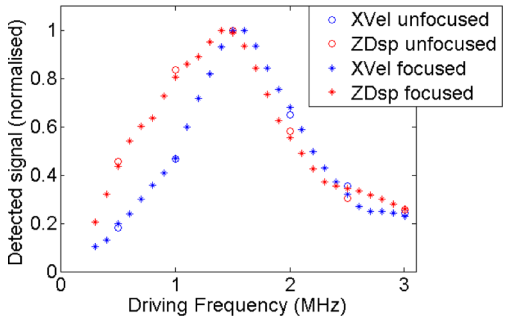

Fig. 19. Maximum peak to peak signal found simulating a racetrack detector at the model centerline as a function of the driving frequency used from a 1.5 mm racetrack spatial profile. XVel indicates the x direction velocity and ZDsp indicates the z, or out-of-plane displacement.

6. Conclusion

A simple analytical solution for the detector coils was presented as an extension from previous work on linear coils [11], which would indicate a peak frequency should be detected at 1.44 MHz. The continuous wave excitation of a racetrack coil can be modeled as a square wave spatial profile, giving an approximate frequency for optimal operation of $0.761v_R/L$. However, data from a variety of 1.5 mm width transmission racetrack EMAT coils showed that experimentally the driving frequency which gives the strongest peak to peak detected signal is lower, ranging from 1.1 to 1.4 MHz. A time evolution model was developed, giving a range of peaks between 1.1 and 1.5 MHz depending on the envelope width of the excitation signal, consistent with the experimental data. The time evolution model predicts minima in the detected signal at every even integer multiple of the wavelength, unless a broadband signal is used. The minima at zero for typical pulse widths shows that racetrack coils act as DC filters. The same model shows that linear coil detectors are more efficient the lower the frequency is, with minima at every integer multiple of the wavelength, unless a broadband signal is used.

It can be concluded that frequency averaging causes the actual frequency peak location for a finite wave packet to ‘blur’ the signal to a slightly lower frequency. Increased coil lift-off has also been shown to lower the central frequency produced by the same coils by 0.06 MHz for a 0.1 mm increase in lift-off, adding to the other effects. Focusing is shown through FEA to have negligible effect on the detected frequencies. The FEA also shows that detected frequencies are dominated by detector effects.

If a coil design needs to be created for a specific frequency of operation then the approximate relation $f_p = 0.761\frac{v}{L}$ can be used to give a rough guide for the optimum frequency of operation for a racetrack coil when long excitation pulses are used. However, if shorter excitation pulses are used the optimum frequency of operation will be lowered. It is recommended that for optimal EMAT signal strengths all coils should be tested with a driving frequency sweep in their desired operation setup to find the exact optimal operation frequency of the whole unit.

Acknowledgements

CBT would like to thank EPSRC and the University of Warwick for funding her PhD studies.

References

[1] H. Hirao, M. Ogi, EMATs for Science and Industry Noncontacting Ultrasonic Measurements, Kluwer Academic Publishers, Boston, 2003.
[2] R.J. Dewhurst, C. Edwards, S.B. Palmer, Appl. Phys. Lett. 49 (7) (1986) 374–376.
[3] X. Jian, I. Baillie, S. Dixon, J. Phys. D: Appl. Phys. 40 (2007) 1501–1506.
[4] P.A. Petcher, M.D.G. Potter, S. Dixon, NDT & E Int. 65 (2014) 1–7.
[5] I. Baillie, P. Griffith, X. Jian, S. Dixon, Insight 49 (2) (2007) 87–92.
[6] N. Lunn, S. Dixon, M.D.G. Potter, NDT & E Int. 89 (2017) 74–80.
[7] S.B. Palmer, S. Dixon, Insight 45 (3) (2003) 211–217.
[8] P. Thayer, Insight 54 (2012) 124–127.
[9] C.B. Thring, Y. Fan, R.S. Edwards, NDT & E Int. 81 (2016) 20–27.
[10] R.S. Edwards, S. Dixon, Ultrasonics 44 (1) (2006) 93–98.
[11] S. Dixon, S.E. Burrows, B. Dutton, Y. Fan, Ultrasonics 51 (1) (2011) 7–16.
[12] G.A. Alers, D.T. Maclauchlan, Rev. Prog. Quant. Nondestruct. Eval. 2A (5) (1983) 271–281.
[13] H. Ogi, M. Hirao, T. Ohtani, IEEE Trans. Ultrason. Ferroelectr. Freq. Control 46 (2) (1999) 341–346.
[14] T. Takishita, K. Ashida, N. Nakamura, H. Ogi, M. Hirao, Jpn. J. Appl. Phys. 54 (7S1) (2015) 07HC04.
[15] S. Wang, R. Su, X. Chen, L. Kang, G. Zhai, IEEE Trans. Ultrason. Ferroelectr. Freq. Control 60 (12) (2013) 2657–2664.
[16] Standard practice for ultrasonic examinations using Electromagnetic Acoustic Transducer (EMAT) techniques, American Society for Testing and Materials, 1996.
[17] P.J. Latimer, D.T. MacLauchlan, EMAT inspection of welds in thin steel plates of dissimilar thicknesses, patent WO1999010737A1, 2000.
[18] P.J. Latimer, D.T. MacLauchlan, EMAT probe and technique for weld inspection, patent US5760307A, 1998.
[19] S. Wang, L. Kang, Z. Li, G. Zhai, L. Zhang, Mechatronics 22 (6) (2012) 653–660.
[20] C.B. Thring, Y. Fan, R.S. Edwards, NDT & E Int. 88 (2017) 1–7.
[21] S. Dixon, S.B. Palmer, Ultrasonics 42 (10) (2004) 1129–1136.
[22] J.P. Morrison, S. Dixon, M.D.G. Potter, X. Jian, Ultrasonics 44 (2006) 1401–1404.
[23] C.V. Dodd, W.E. Deeds, J. Appl. Phys. 39 (6) (1968) 2829–2838.
[24] S. Dixon, T.J. Harrison, P.A. Petcher, Appl. Phys. Lett. 97 (5) (2010) 2008–2010.
[25] L.G. Gouy, C.R. Acad, Sci. Paris 110 (1890) 1251.